A VCP inhibitor substrate trapping approach (VISTA) enables proteomic profiling of endogenous ERAD substrates

Edmond Y. Huang[a,†], Milton To[a,†], Erica Tran[a], Lorraine T. Ador Dionisio[a], Hyejin J. Cho[a], Katherine L. M. Baney[a], Camille I. Pataki[b], and James A. Olzmann[a,*]

[a]Department of Nutritional Sciences and Toxicology, University of California, Berkeley, Berkeley, CA 94720; [b]Biomedical Informatics Program, Stanford University, Stanford, CA 94305

ABSTRACT **Endoplasmic reticulum (ER)–associated degradation (ERAD) mediates the proteasomal clearance of proteins from the early secretory pathway. In this process, ubiquitinated substrates are extracted from membrane-embedded dislocation complexes by the AAA ATPase VCP and targeted to the cytosolic 26S proteasome. In addition to its well-established role in the degradation of misfolded proteins, ERAD also regulates the abundance of key proteins such as enzymes involved in cholesterol synthesis. However, due to the lack of generalizable methods, our understanding of the scope of proteins targeted by ERAD remains limited. To overcome this obstacle, we developed a VCP inhibitor substrate trapping approach (VISTA) to identify endogenous ERAD substrates. VISTA exploits the small-molecule VCP inhibitor CB5083 to trap ERAD substrates in a membrane-associated, ubiquitinated form. This strategy, coupled with quantitative ubiquitin proteomics, identified previously validated (e.g., ApoB100, Insig2, and DHCR7) and novel (e.g., SCD1 and RNF5) ERAD substrates in cultured human hepatocellular carcinoma cells. Moreover, our results indicate that RNF5 autoubiquitination on multiple lysine residues targets it for ubiquitin and VCP-dependent clearance. Thus, VISTA provides a generalizable discovery method that expands the available toolbox of strategies to elucidate the ERAD substrate landscape.**

Monitoring Editor
Thomas Sommer
Max Delbrück Center for Molecular Medicine

Received: Aug 16, 2017
Revised: Feb 5, 2018
Accepted: Feb 26, 2018

This article was published online ahead of print in MBoC in Press (http://www.molbiolcell.org/cgi/doi/10.1091/mbc.E17-08-0514) on March 5, 2018.

†These authors contributed equally.

*Address correspondence to: James A. Olzmann (olzmann@berkeley.edu).

Abbreviations used: AAA, ATPases associated with diverse cellular activities; AP, affinity purification; ApoB100, apolipoprotein B100; ATP, adenosine triphosphate; AU, arbitrary units; Btz, bortezomib; CG, core glycosylated; CRISPR, clustered regularly interspaced short palindromic repeats; DAVID, Database for Annotation, Visualization and Integrated Discovery; DHCR7, 7-dehydrocholesterol reductase; diGly, diglycine; ER, endoplasmic reticulum; ERAD, ER-associated degradation; GFP, green fluorescent protein; GO, gene ontology; HMG CoA reductase, 3-hydroxy-3-methylglutaryl-coenzyme A reductase; Insig, insulin-induced gene; IP, immunoprecipitation; IP3, inositol triphosphate; KO, knockout; MBP, maltose-binding protein; NEM, *N*-ethylmaleimide; NHK, null Hong Kong; RPMI, Roswell Park Memorial Institute; SCD, stearoyl-CoA desaturase; SILAC, stable isotope labeling with amino acids in cell culture; TM, transmembrane domain; TSC, total spectral counts; VCP, valosin containing protein; VISTA, VCP inhibitor substrate trapping approach; WT, wild type.

INTRODUCTION

The endoplasmic reticulum (ER) mediates the folding, modification, and deployment of one-third of the cellular proteome. Proteins that fail to fold or lack requisite oligomeric binding partners are degraded through ER-associated degradation (ERAD), a ubiquitin-dependent process that targets substrates to the 26S proteasome for proteolysis (Olzmann *et al.*, 2013; Christianson and Ye, 2014; Ruggiano *et al.*, 2014). A modular network of ERAD machinery coordinates substrate recognition and dislocation (also known as retrotranslocation) from the ER lumen or membrane into the cytoplasm (Carvalho *et al.*, 2006; Christianson *et al.*, 2011). ER-resident E3 ubiquitin ligases mediate substrate ubiquitination, which serves both as a proteasomal targeting signal and a binding interface that facilitates substrate extraction by the homohexameric AAA ATPase VCP (also known as p97) and its associated ubiquitin-binding cofactors (e.g., UFD1L and NPLOC4; Olzmann *et al.*, 2013; Ye *et al.*, 2017). VCP-mediated ATP hydrolysis generates the necessary force for the extraction of the ubiquitinated substrate, which is partially unfolded as it is threaded through the VCP central pore (Ernst *et al.*, 2011; Blythe *et al.*, 2017; Bodnar and Rapoport, 2017).

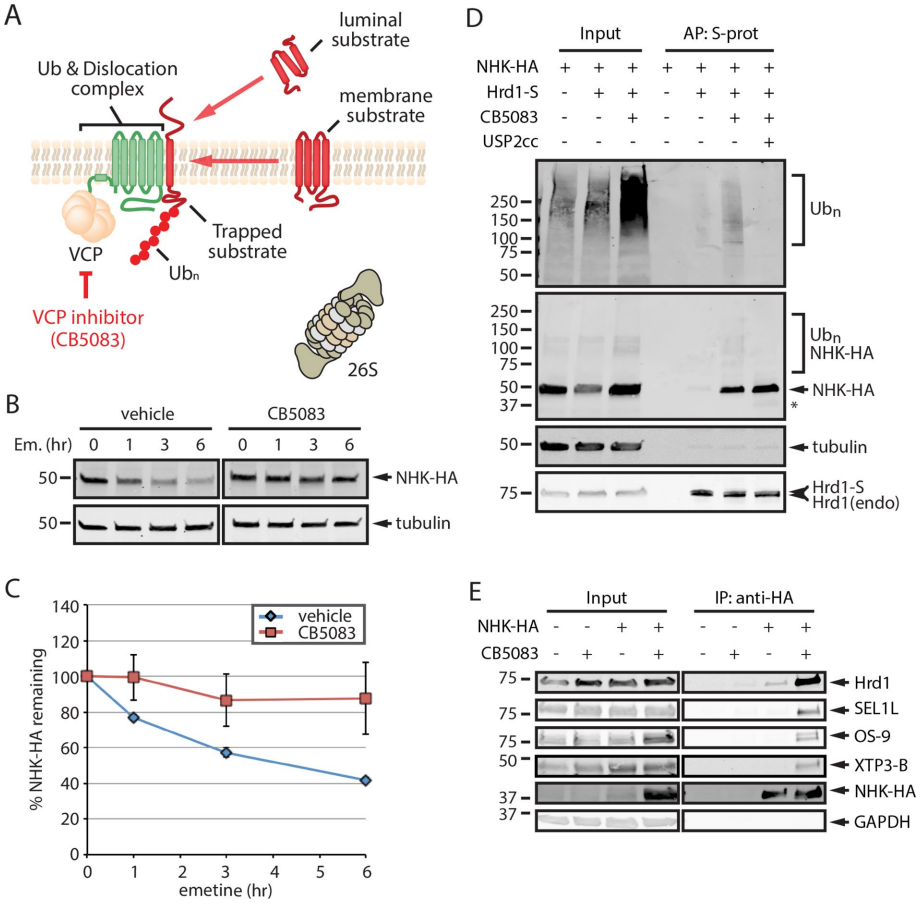

FIGURE 1: VCP inhibition traps the ERAD substrate NHK in complex with the E3 ligase Hrd1. (A) Schematic of VISTA. Pharmacological inhibition of VCP with CB5083 prevents the dislocation of ubiquitinated ERAD substrates. (B) HEK293 cells expressing NHK-HA were incubated with 75 μM emetine and either vehicle or 5 μM CB5083 for the indicated time points. SDS lysates were analyzed by immunoblotting for the indicated targets. (C) The relative levels of NHK-HA (panel B) were quantified and presented as a percentage of the levels at time 0 h ± SEM ($n = 3$). (D) HEK293 cells stably expressing Hrd1-S were transiently transfected with NHK-HA, treated with vehicle or 5 μM CB5083, subject to affinity purification with S-protein (S-prot) agarose, and SDS lysates analyzed by immunoblotting; $n = 3$. (E) HEK293 cells stably expressing NHK-HA were treated with vehicle or 5 μM CB5083, subject to affinity purification with anti-HA–conjugated agarose, and SDS lysates analyzed by immunoblotting. Asterisk indicates a USP2cc-reactive band. AP, affinity purification; IP, immunoprecipitation; S-prot, S-protein; Ubn, ubiquitinated; endo, endogenous; Em., emetine.

A canonical role of ERAD is the clearance of misfolded proteins (i.e., quality control), such as the ΔF508 mutant cystic fibrosis transmembrane conductance regulator in cystic fibrosis and the truncated null Hong Kong (NHK) variant of α-1 antitrypsin in α-1 antitrypsin deficiency (Guerriero and Brodsky, 2012). The identification of disease-associated mutant proteins as ERAD substrates has provided useful tools to study the mechanisms of ERAD (Needham and Brodsky, 2013). A less appreciated role of ERAD is in regulating the levels of endogenous proteins (i.e., quantity control; Hegde and Ploegh, 2010; Stevenson *et al.*, 2016; Qi *et al.*, 2017**).** For example, ERAD controls the flux through the cholesterol synthesis pathway by facilitating the sterol-regulated degradation of HMG CoA reductase (Song *et al.*, 2005) and squalene monooxygenase (Gill *et al.*, 2011; Foresti *et al.*, 2013). ERAD quantity control has also been implicated in a wide variety of pathological conditions, such as cancer, hepatic steatosis, obesity, diabetes insipidus, and immune system function, through its ability to degrade ER-resident proteins (e.g., HMG CoA reductase, Insig1/2), secreted proteins (e.g., ApoB100, proAVP), and plasma membrane proteins (e.g., KAI1, CD147, pre–B cell receptor, SLC1A5, SLC38A2; Song *et al.*, 2005; Lee *et al.*, 2006; Tsai *et al.*, 2007; Liu *et al.*, 2012; Tyler *et al.*, 2012; Fisher *et al.*, 2014; Jeon *et al.*, 2015; Ji *et al.*, 2016; Shi *et al.*, 2017; To *et al.*, 2017). Thus, by influencing the abundance of ER-resident proteins and secreted proteins, ERAD impacts both cell autonomous and noncell autonomous processes.

Despite the importance of ERAD in protein quantity control, our understanding of the endogenous substrates targeted by ERAD remains limited. This surprising dearth of knowledge is in part due to the lack of generalizable methods to identify endogenous ERAD substrates in human cells. Here, we describe a quantitative ubiquitin proteomics strategy termed VCP inhibitor substrate trapping approach (VISTA) to identify endogenous ERAD substrates.

RESULTS AND DISCUSSION

VCP inhibition traps ubiquitinated NHK in complex with the Hrd1 E3 ubiquitin ligase

A principal function of VCP is to extract ubiquitinated ERAD substrates from the ER into the cytosol for proteasomal degradation (Bagola *et al.*, 2011; Ye *et al.*, 2017). CB5083 is a small-molecule VCP inhibitor that impairs the degradation of several integral membrane ERAD substrates, including CD147 (To *et al.*, 2017), c18orf32 (Bersuker *et al.*, 2018), and overexpressed TCRα-GFP (Anderson *et al.*, 2015). In addition, incubation with CB5083 results in the accumulation of ubiquitinated proteins (Anderson *et al.*, 2015; Gendron *et al.*, 2016). We reasoned that acute pharmacological inhibition of VCP with CB5083 could be exploited to stabilize or "trap" ERAD substrates in a ubiquitinated, membrane-bound form (Figure 1A).

As a first test of the utility of CB5083 to trap ERAD substrates, we examined the impact of CB5083 treatment on the well-characterized luminal ERAD substrate NHK. In a translation shut-off assay, the half-life HA-tagged NHK (NHK-HA) was greatly extended in the presence of CB5083 (Figure 1, B and C), demonstrating that incubation with CB5083 impairs the degradation of a luminal ERAD substrate. Dislocation and ubiquitination of NHK are mediated by a membrane-embedded, macromolecular complex containing the E3 ubiquitin ligase Hrd1 (Christianson *et al.*, 2008; Hosokawa *et al.*, 2008). Thus, we sought to test the hypothesis that VCP inhibition traps polyubiquitinated NHK in complex with Hrd1. CB5083 treatment led to both an increase in ubiquitinated proteins in cell lysates (i.e., Input) as well as an increased association of NHK-HA and ubiquitinated proteins with S-tagged Hrd1 (Hrd1-S), consistent with impaired clearance of ubiquitin-conjugated proteins (Figure 1D). A portion of NHK-HA associated with Hrd1-S migrated as a high-molecular-weight smear that was sensitive to incubation with the

catalytic core of the deubiquitinating enzyme USP2 (USP2cc; Figure 1D), indicating that this fraction of NHK-HA in complex with Hrd1-S is ubiquitinated. Furthermore, immunoprecipitations of NHK-HA indicate that CB5083 increases the association of NHK-HA with components of the Hrd1 complex, including Hrd1, SEL1L, OS-9, and XTP3-B (Figure 1E). These proof-of-principle experiments demonstrate that CB5083 treatment traps a known ERAD substrate in a ubiquitinated form, in complex with its membrane-embedded degradation apparatus. We also observed that CB5083 treatment resulted in the accumulation of the core glycosylated form of integral membrane protein CD147 (CD147[CG]), an endogenous ERAD substrate (Tyler *et al.*, 2012; To *et al.*, 2017), but it caused only a small increase in the association of CD147(CG) with Hrd1-S (Supplemental Figure S1). This may reflect differences in the mode of interaction between Hrd1 and its luminal and integral membrane substrates. For example, under periods of VCP impairment, an integral membrane substrate may be preferentially released into the surrounding membrane to prevent prolonged occupancy of the Hrd1 ubiquitination complex.

Global analysis of trapped, ubiquitinated proteins identifies endogenous ERAD substrates in HepG2 liver cells

To identify endogenous ERAD substrates, VCP inhibition was coupled with quantitative ubiquitin proteomics in a method we refer to as ERAD-VISTA (Figure 2A). Cells were labeled by stable isotope labeling with amino acids in cell culture (SILAC) and treated with vehicle (light) or CB5083 (heavy). Beads conjugated with antibodies that recognize peptides bearing diglycine (diGly)-modified lysine residues (i.e., a tryptic ubiquitin remnant; Kim *et al.*, 2011; Gendron *et al.*, 2016) were used to affinity purify ubiquitin-modified peptides from membrane fractions for proteomic analysis. Consistent with the trapping of ubiquitinated proteins, CB5083 treatment resulted in greater levels of polyubiquitinated proteins in cell lysate and the ER-enriched membrane fraction (Figure 2B). Proteomic analysis of diGly-modified peptides purified from membrane fractions identified a total of 5573 diGly-modified peptides across four independent experiments, corresponding to 478 proteins (Supplemental Table S1). There was some variability in the number of unique diGly peptides identified (Figure 2C and Supplemental Table S1), which may be due to different batches of diGly beads. Experiments 3 and 4 were performed with the same batch of beads and were very similar with respect to the number of unique diGly peptides identified in each experiment (Figure 2C and Supplemental Table S1). diGly-modified peptides with SILAC ratios greater than 2.0 (123 proteins), indicating an accumulation of the ubiquitinated peptide during VCP inhibition, were considered candidate ERAD substrates (Supplemental Figure S2 and Supplemental Table S1). A single diGly modification was identified for the majority of proteins (68.2% for all proteins, 59.2% for proteins with SILAC ratio > 2), but a fraction of the proteins were also observed that contained two diGly modifications (18.8% for all proteins, 20.8% for proteins with SILAC ratio > 2) or three diGly modifications (9.6% for all proteins, 12.5% for proteins with SILAC ratio > 2; Figure 2D). As expected, a large number of ubiquitin diGly peptides were identified, most of which corresponded to K48 and K63 diGly-modified peptides (Figure 2E). In all four experiments, K11, K33, and K48 diGly peptides showed a strong increase, consistent with a role in protein degradation (Figure 2F). In contrast, the amount of K63 diGly peptide was mostly unchanged and the amount of K27 diGly peptide showed a decrease (Figure 2F).

Among the list of candidate substrates (Supplemental Table S1), three bona fide endogenous ERAD substrates were detected: Apolipoprotein B100 (ApoB100; Ginsberg and Fisher, 2009; Stevenson *et al.*, 2016), 7-dehydrocholesterol reductase (DHCR7; Prabhu *et al.*, 2016), and insulin-induced gene 2 (Insig2; Liu *et al.*, 2012). Following CB5083 treatment, increases in the levels of two diGly peptides in ApoB100 (K196, 13.805-fold increase; K2697, 9.249-fold increase), a cluster of three diGly peptides in DHCR7 (K4, 3.602-fold increase; K11, 3.497-fold increase; K13, 3.861-fold increase), and one diGly peptide in Insig2 (K221, 7.27-fold increase) were detected (Figure 2, G–L), suggesting that modification of these lysines by ERAD E3 ligases targets these substrates to the proteasome. Other reported endogenous ERAD substrates may not have been identified due to their low abundance in HepG2 cells or their regulated degradation under specific conditions, such as IP3 receptor degradation following ligand binding (Wojcikiewicz *et al.*, 2009) or HMG CoA reductase degradation following sterol accumulation in ER membranes (Jo and Debose-Boyd, 2010). Although it is unlikely to be a comprehensive list, these data demonstrate the ability of ERAD-VISTA to detect known and candidate endogenous ERAD substrates.

Gene ontology (GO) enrichment analysis of candidate ERAD substrates revealed an expected enrichment in proteins that are known to localize to cell membranes (e.g., ER and plasma membrane) as well as complexes associated with various components of the ERAD network (Figure 3A and Supplemental Table S2). Indeed, analysis of the annotated localizations revealed that 59.2% of the candidate substrates were predicted to be present in, or transit through, the secretory pathway (Supplemental Table S3). A smaller portion of the candidate substrates are annotated as mitochondrial (8.3%), lysosomal (0.8%), and vesicular (1.7%; Supplemental Table S3), indicating a high degree of enrichment in ubiquitinated secretory proteins. We observed an enrichment in proteins involved amino acid transport, protein catabolism, protein folding, and cholesterol and fatty acid biosynthesis (Figure 3B and Supplemental Table S2). This functional diversity reflects the wide array of potential ERAD substrates transiting the early secretory pathway and is consistent with a broad cellular role for ERAD through its regulation of a multitude of targets.

Degradation of endogenous SCD1 and RNF5 requires VCP, ubiquitin conjugation, and the proteasome

We next sought to validate select putative ERAD substrates from our candidate list. Two candidate substrates were selected for further analysis. Stearoyl-CoA desaturase (SCD1) is an ER-localized enzyme that catalyzes the production of monounsaturated fatty acids from saturated fatty acids (Ntambi and Miyazaki, 2003). Levels of a diGly-modified lysine in the cytosolic C-terminus of SCD1 increased in response to CB5083 (K341, 10.621-fold increase; Figure 4, A and B). Overexpressed SCD1 in CHO-K1 and HeLa cells as well as endogenous SCD1 in NIH3T3-L1 cells are degraded by the proteasome (Mziaut *et al.*, 2000; Kato *et al.*, 2006). However, whether VCP is required for SCD1 degradation and whether endogenous SCD1 is degraded in HepG2 cells remains unknown. Consistent with SCD1 being a direct substrate of VCP, CB5083 treatment increased the amount of VCP associated with S-tagged SCD1 (SCD1-S; Figure 4C). Moreover, the degradation of SCD1 was impaired by CB5083, the proteasome inhibitor MG132, and an inhibitor of the E1 ubiquitin-activating enzyme MLN7243 (Figure 4, D and E). We observed an anti-SCD1 immunoreactive, lower-molecular-weight band that was partially degraded in control cells and exhibited a modest accumulation in the presence of the inhibitors (Figure 4D). This band was depleted by multiple small interfering RNAs (siRNAs) targeting SCD1 (Supplemental Figure S3), confirming that it is a fragment of SCD1, but its functional significance is

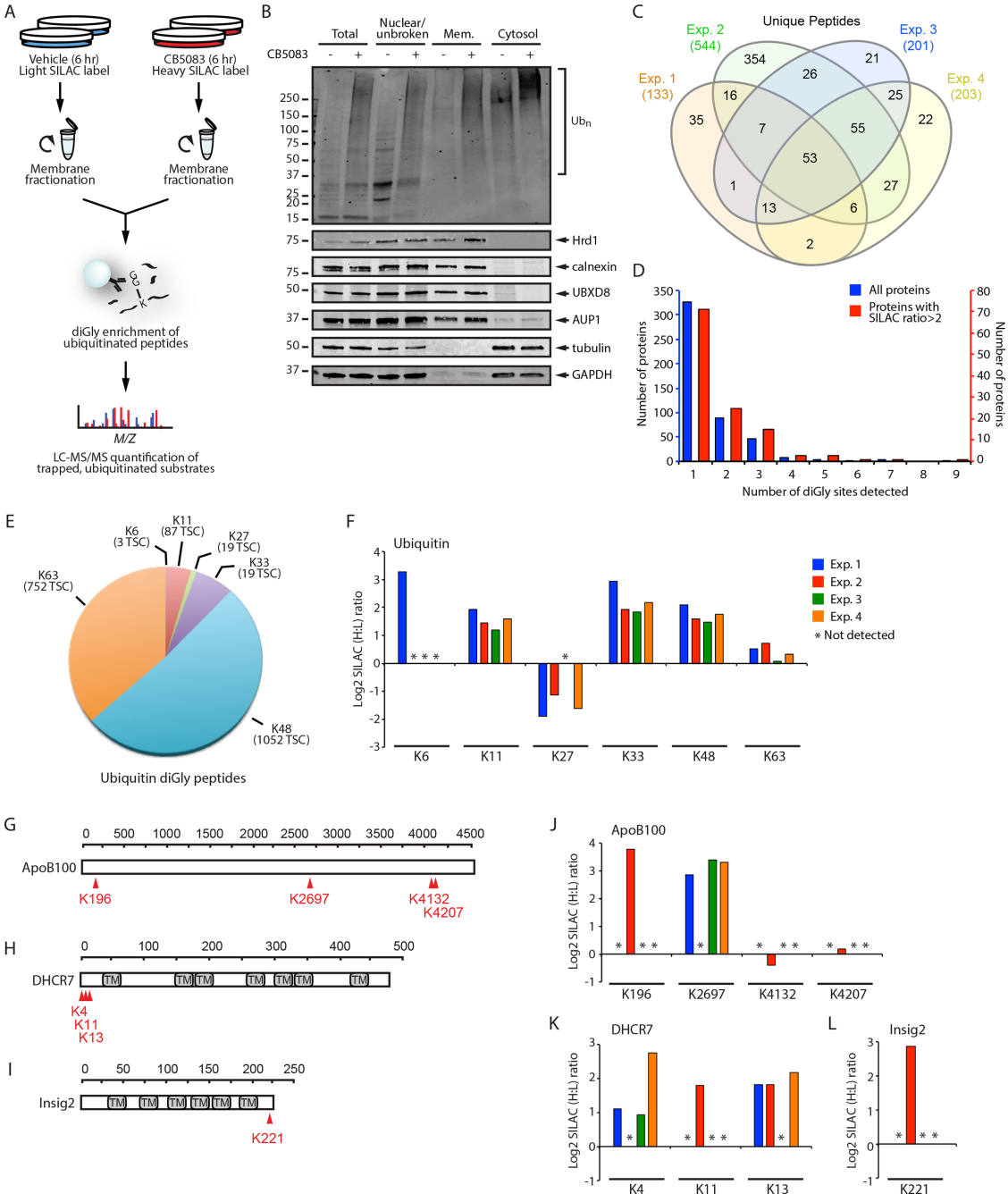

FIGURE 2: Global analysis of trapped, ubiquitinated proteins identifies validated and candidate ERAD substrates in cultured liver cells. (A) Schematic of ERAD-VISTA experimental workflow. (B) HepG2 cells treated with vehicle or 5 μM CB5083 were fractionated by differential centrifugation and equal volumes analyzed by immunoblotting; $n = 3$. (C) Venn diagram comparing unique diGly-modified peptides identified from the four independent experiments. (D) Bar graph indicating the number of unique diGly sites identified for all proteins (blue) and for proteins with a SILAC ratio > 2 (red). (E) Pie chart illustrating the relative abundance of diGly-modified ubiquitin peptides, based on total spectral counts. (F) Log2 SILAC peptide ratios for individual diGly-modified peptides from ubiquitin. (G–I) Protein domain structure and the identified diGly-modified lysine residues for three validated endogenous ERAD substrates (ApoB100, DHCR7, and Insig2). TM: transmembrane domain. (J–L) Log2 SILAC peptide ratios for individual diGly-modified peptides from ApoB100 (J), DHCR7 (K), and Insig2 (L). Colors indicate the experiment from which the diGly peptide was identified, as in panel F. Mem., membrane; Ubn, ubiquitinated; Exp., experiment; TSC, total spectral counts. Asterisk indicates that the diGly peptide was not detected in that experiment. See also Supplemental Table S1.

unclear at this time. Our data suggest that SCD1 is constitutively degraded by a VCP-dependent ERAD pathway in HepG2 cells. This is similar to the SCD1 yeast orthologue OLE1, which undergoes degradation through an ERAD pathway that requires the VCP orthologue CDC48 (Braun *et al.*, 2002). Future experiments will explore if SCD1 degradation is regulated by the metabolic state of the cell, such as fluctuations in the ratio of unsaturated to saturated fatty acids.

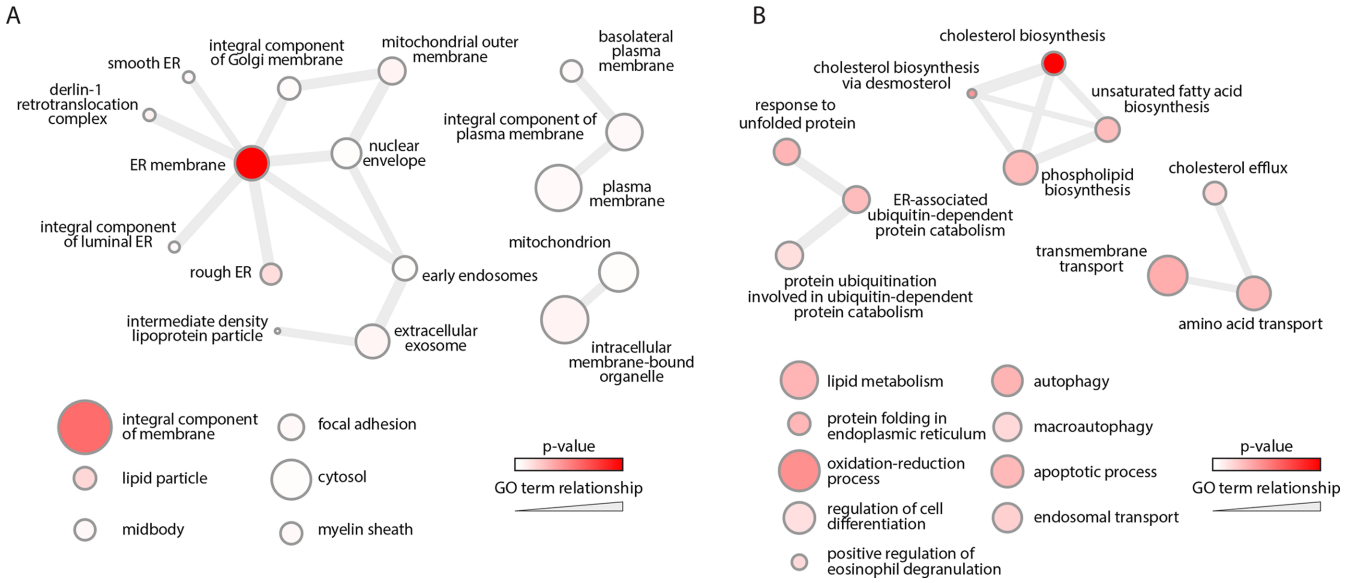

FIGURE 3: Gene ontology analysis of candidate ERAD substrates. (A, B) DAVID and REVIGO were used to identify enriched GO terms, cellular component (A) or biological function (B), within the candidate ERAD substrate list. Cytoscape networks were generated by REVIGO. Circle size indicates the frequency of the GO term in the GO annotation database, edge thickness is proportional to the degree of GO term similarity, and color indicates the *p* value (red being more significant). See also Supplemental Table S2.

Another candidate ERAD substrate identified using VISTA is RNF5, an ERAD E3 ligase that mediates the clearance of misfolded proteins (Younger *et al.*, 2006; Morito *et al.*, 2008; Grove *et al.*, 2011) and controls the stability of proteins involved in a variety of cellular processes such as autophagy (Kuang *et al.*, 2012), amino acid transport (Jeon *et al.*, 2015), and viral immunity (Zhong *et al.*, 2010). We identified four diGly-modified lysines that clustered within the cytosolic N-terminus of RNF5 and increased following CB5083 treatment (K68, 4.029-fold increase; K75, 7.038-fold increase; K86, 6.307-fold increase; K93, 8.339-fold increase; Figure 4, F and G). Similar to SCD1-S, CB5083 treatment increased the amount of VCP that coprecipitated with S-RNF5 (Figure 4H). Translation shut-off experiments indicated that the degradation of endogenous RNF5 was impaired by CB5083, MG132, and MLN7243 (Figure 4, I and J). Together, our findings indicate that two of the candidate ERAD substrates in HepG2 cells identified by ERAD-VISTA, SCD1 and RNF5, are constitutively degraded by a VCP- and ubiquitin-dependent ERAD pathway.

Autoubiquitination targets RNF5 to the ERAD pathway in HepG2 cells

Maltose-binding protein (MBP)–tagged RNF5 autoubiquitinates in vitro through an intramolecular reaction that requires an intact RING finger domain (Matsuda *et al.*, 2001). However, whether RNF5 autoubiquitinates in cells and whether this activity contributes to its proteasomal clearance has not been examined. We generated an S-tagged RNF5 construct containing a cysteine-to-alanine substitution (C42A), which disrupts the RING finger and abrogates its catalytic activity (Matsuda *et al.*, 2001). When transfected into HepG2 cells, S-RNF5(WT) overexpression was low (Supplemental Figure S4A) and the S-RNF5(C42A) exhibited a threefold increase in protein levels relative to its wild-type counterpart (Figure 5, A and B). Inhibitors of ERAD increased the steady-state levels of wild-type RNF5, but not S-RNF5(C42A) (Figure 5, A and B), indicating that RNF5 ubiquitination activity is required for its degradation. Affinity purification of S-RNF5(WT) revealed a laddering of RNF5 bands, with three to four particularly prominent bands that were separated by ~8 kDa (i.e., the size of ubiquitin) and that increased following CB5083 treatment (Figure 5, C and D). These bands were greatly reduced by incubation with USP2cc, indicating that these represent ubiquitinated forms of RNF5 (Figure 5, C and D). The ubiquitinated RNF5 species were mostly absent in the C42A mutant RNF5 (Figure 5, C and D). We considered that the small amount of ubiquitinated S-RNF5(C42A) may be due to ubiquitination S-RNF5(C42A) by endogenous RNF5. Indeed, FLAG-HA-RNF5 coprecipitated with S-RNF5, indicating the presence of RNF5 homo-oligomers (Supplemental Figure S4B). To examine the possibility of *trans*-molecular RNF5 autoubiquitination, we expressed S-RNF5(C42A) in RNF5 knockout (KO) cells generated using CRISPR/Cas9 (Supplemental Figure S5). Similar to the control cells, S-RNF5(C42A) still exhibited a small amount of laddering in the RNF5 KO cells, indicating that the endogenous RNF5 does not contribute to the ubiquitination of S-RNF5(C42A) (Supplemental Figure S5B). Our data are in very good agreement with previous in vitro studies (Matsuda *et al.*, 2001) and suggest RNF5 autoubiquitination is a *cis*-molecular reaction. The residual ubiquitination of S-RNF5(C42A) must be mediated by an unknown E3 ligase.

Our proteomics results indicate that all four lysines in RNF5 are ubiquitinated and are sensitive to VCP inhibition (Figure 4, F and G, and Supplemental Table S1). To explore the contribution of these lysines to RNF5 degradation we generated constructs harboring lysine-to-arginine substitutions. Although there was a small decrease in the ubiquitination of S-RNF5(K75R) and S-RNF(K86R), all S-RNF5 single lysine mutants were still ubiquitinated (Figure 5E). Therefore, we generated an S-RNF5 construct in which all four lysines were substituted with arginine (4K-R). The 4K-R mutant exhibited a dramatic reduction in ubiquitination (Figure 5, F and G). A very small amount of ubiquitinated S-RNF5(4K-R) was visible, suggesting that RNF5 may either ubiquitinate noncanonical residues (e.g., serine) or one of the lysines in the S-tag. Although the S-tag contains two lysine residues, the ubiquitination of RNF5 was nearly abolished in the 4K-R mutant. This may indicate a structural preference for the

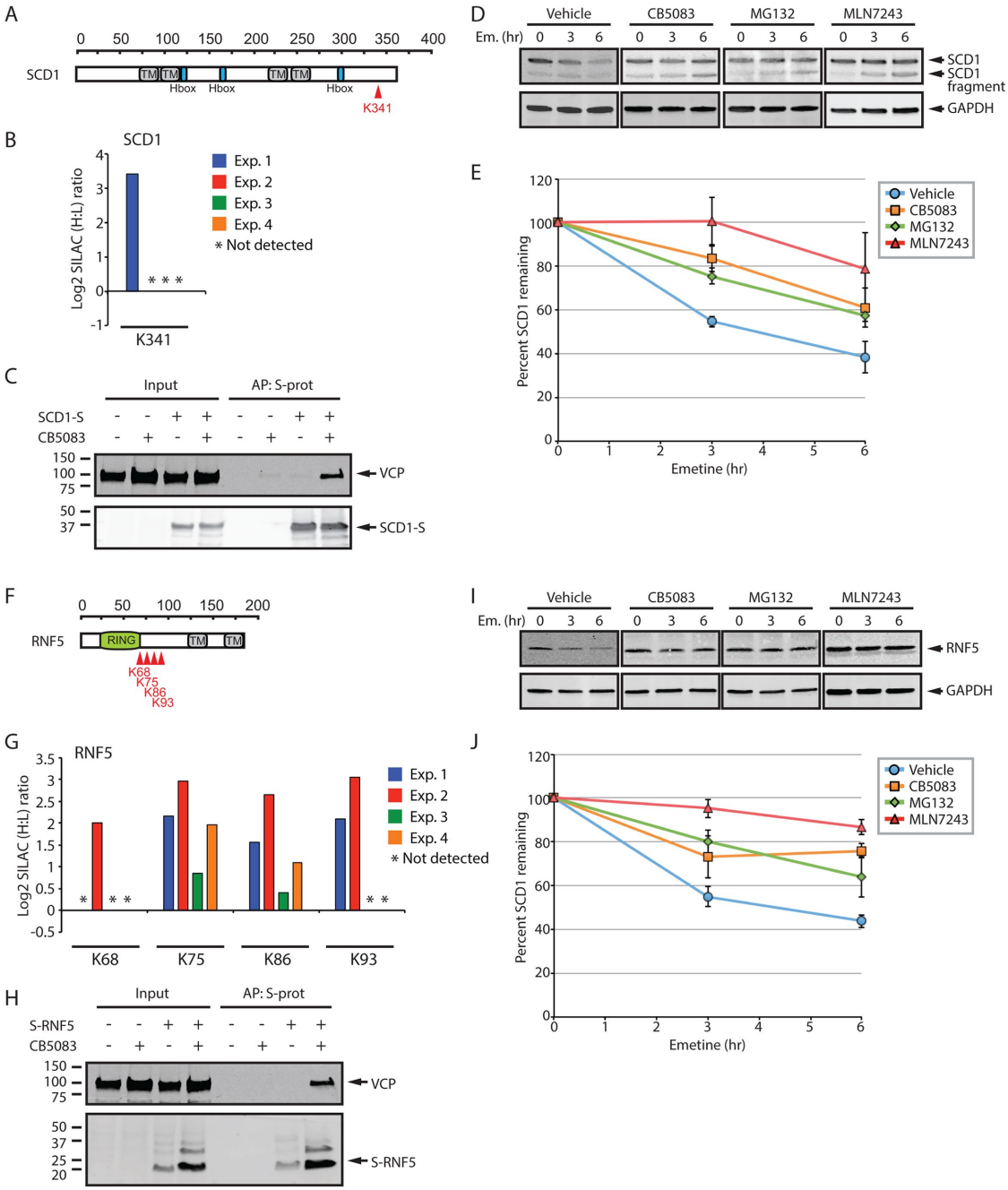

FIGURE 4: Endogenous SCD1 and RNF5 are degraded via a VCP- and ubiquitin-dependent proteasomal pathway. (A) Diagram of SCD1 protein structure, with detected diGly-modified lysine residue indicated. (B) Log2 SILAC peptide ratios for individual diGly-modified peptides from SCD1. (C) HepG2 cells expressing SCD1-S were treated with vehicle or 5 μM CB5083, subject to affinity purification with S-protein (S-prot) agarose, and SDS lysates analyzed by immunoblotting; $n = 3$. (D, E) HepG2 cells were treated with 75 μM emetine and 5 μM CB5083, 10 μM MG132, or 10 μM MLN7243 to disrupt various components of ERAD. SCD1 protein stability was assessed via immunoblotting (D) and relative levels quantified (E). Graphical data are expressed as mean ± SEM ($n = 3$–6 per group). (F) Diagram of RNF5 protein structure, with detected diGly-modified lysine residues indicated. (G) Log2 SILAC peptide ratios for individual diGly-modified peptides from RNF5. (H) HepG2 cells expressing S-RNF5 were treated with vehicle or 5 μM CB5083, subject to affinity purification with S-protein (agarose, and SDS lysates analyzed by immunoblotting) ($n = 3$). (I, J) HepG2 cells were treated with 75 μM emetine and 5 μM CB5083, 10 μM MG132, or 10 μM MLN7243 to disrupt various components of ERAD. RNF5 protein stability was assessed via immunoblotting (I) and relative levels quantified (J). Graphical data are expressed as mean ± SEM ($n = 3$–6 per group). TM: transmembrane domain. S-prot, S-protein; Exp., experiment; Em., emetine. Asterisk indicates that the diGly peptide was not detected in that experiment. See also Supplemental Table S1.

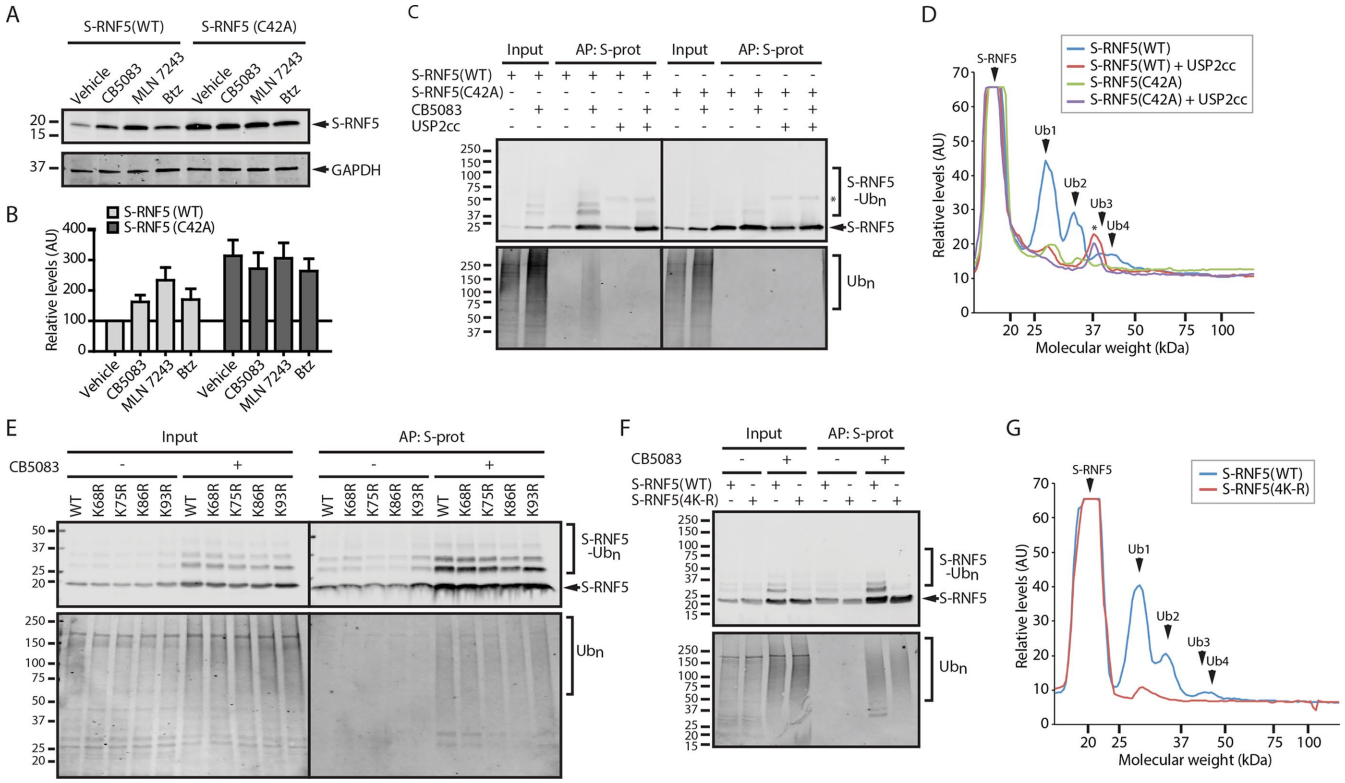

FIGURE 5: RNF5 autoubiquitination targets it for ERAD. (A) HepG2 cells transfected with S-RNF5(WT) and S-RNF5(C42A) were treated as indicated and lysates analyzed by immunoblotting. (B) Densitometric quantification of S-RNF5 (panel A). Data are expressed as mean ± SEM ($n = 4$ per group). (C) HepG2 cells transfected with S-RNF5(WT) and S-RNF5(C42A) were treated for 6 h with vehicle or 5 μM CB5083. S-tagged proteins were affinity purified, incubated in the presence and absence of USP2cc, and analyzed by immunoblotting. (D) Densitometric quantification of S-RNF5 (panel C). (E) HepG2 cells expressing S-RNF5(WT) or S-RNF5(C42A) were treated for 6 h with vehicle or 5 μM CB5083. S-tagged proteins were affinity purified, incubated in the presence or absence of USP2cc, and analyzed by immunoblotting. (F) HepG2 cells expressing S-RNF5(WT) or S-RNF5(4K-R) were treated for 6 h with vehicle or 5 μM CB5083. S-tagged proteins were affinity purified, incubated in the presence or absence of USP2cc, and analyzed by immunoblotting. (G) Densitometric quantification of S-RNF5 affinity purified from CB5083 treated HepG2 cells (panel F). Btz: bortezomib; Ubn, ubiquitinated; S-prot, S-protein. AU: arbitrary units. Asterisk indicates a USP2cc-reactive band.

cluster of 4-lysine residues over the lysines in the N-terminal S-tag. It is notable that S-RNF5(4K-R), despite being no longer ubiquitinated, still coprecipitated ubiquitinated proteins in the presence of CB5083 (Figure 5F). This was in contrast to the inactive S-RNF5(C42A), which did not coprecipitate ubiquitinated proteins (Figure 5C). These results suggest that the S-RNF5(4K-R) mutant uncouples RNF5 catalytic activity and autoubiquitination. This uncoupling mutant could be useful for exploring the functional importance of RNF5 degradation.

In summary, we have developed a new global approach for the identification of endogenous ERAD substrates. This approach identified known (ApoB100, DHCR7, and Insig2) and novel (SCD1 and RNF5) substrates. ERAD-VISTA has several important benefits over previous strategies to study ubiquitinated substrates: 1) The method uses endogenous ubiquitin and does not require overexpression of tagged ubiquitin (e.g., his-ubiquitin [Hitchcock *et al.*, 2003; Peng *et al.*, 2003; Kirkpatrick *et al.*, 2005]). 2) The method does not require in-depth knowledge and/or genetic manipulation of the degradation pathway (e.g., proteomic analyses of tagged E3 ligase complexes [Gao *et al.*, 2011; Tan *et al.*, 2011, 2013; Harper and Tan, 2012] or tagged substrate delivery factors [Tyler *et al.*, 2012]). 3) The method does not require expression of chimeric proteins that could affect function (e.g., fusions of E3 ligases to tandem ubiquitin-binding domains [Mark *et al.*, 2014, 2016] or to ubiquitin [O'Connor *et al.*, 2015]). 4) The method measures changes in substrate ubiquitination rather than steady-state protein levels (e.g., steady-state SILAC [Foresti *et al.*, 2014] or GFP-based global protein profiling [Yen and Elledge, 2008; Yen *et al.*, 2008]), thereby facilitating substrate identification even when only a small fraction is ubiquitinated and degraded. A limitation of ERAD-VISTA is that it relies on diGly ubiquitin proteomics which may impact reproducibility due to stochastic sampling, especially for low-abundance targets (Ordureau *et al.*, 2015). Thus, achieving comprehensive assessments of the ERAD substrate landscape is a challenge. However, depth and coverage may be improved by employing recent improvements in diGly methodologies involving the fractionation of peptides using strong cation exchange chromatography before immunoaffinity purification (Na *et al.*, 2012; Udeshi *et al.*, 2012). It is also important to note that because the diGly approach is specific to diGly-modified lysines, it will not identify ubiquitination on nonlysine residues such as serine (Shimizu *et al.*, 2010). An additional limitation of ERAD-VISTA is that some CB5083-sensitive ubiquitination events might not target the modified protein for degradation and may instead reflect regulatory ubiquitination, such as the ubiquitin-dependent regulation of protein

complexes (Hoppe *et al.*, 2000; Rape *et al.*, 2001; Ramanathan and Ye, 2012). Thus, the candidate ERAD substrate must be validated with traditional approaches. ERAD-VISTA expands the available toolbox of strategies for probing the ERAD substrate landscape in different cell types and under different conditions (e.g., ER stress).

MATERIALS AND METHODS

Plasmids, antibodies, and reagents

The NHK-HA and Hrd1-S plasmids used were previously described (To *et al.*, 2017). The S-RNF5 plasmid in a pcDNA3.1(+) backbone was a kind gift from Ron Kopito (Stanford University), and the FLAG-HA-RNF5 plasmid in a pcDNA5/FRT/TO backbone was a kind gift from John Christianson (Ludwig Institute for Cancer Research, University of Oxford). S-RNF5 lysine-to-arginine and cysteine-to-alanine substitutions were generated by site-directed mutagenesis and confirmed by sequencing. To generate the SCD1-S expression plasmid, SCD1 was PCR amplified from pANT7_cGST-SCD1 (DNASU Plasmid Repository, HsCD00631016) and ligated into a pcDNA3.1(–) vector bearing an in frame C-terminal S-tag.

The primary antibodies used for immunoblotting include anti-S peptide (EMD Millipore), anti-HA (Sigma-Aldrich), anti-ubiquitin (FK2; EMD Millipore), anti-tubulin (Abcam), anti-Hrd1 (Bethyl Laboratories), anti-SEL1L (Santa Cruz), anti-CD147 (Santa Cruz), anti-VCP (Novus Biologicals), anti-calnexin (Proteintech Group), anti-UBXD8 (Proteintech Group), anti-AUP1 (Proteintech Group), anti-GAPDH (EMD Millipore), anti-SCD1 (Cell Signaling Technology), and anti-RNF5 (Abcam). Anti-OS-9 and anti-XTP3-B were kind gifts from Ron Kopito (Stanford University). Secondary antibodies used were Alexa Fluor 680 goat anti-mouse (Life Technologies) and IRDye 800 goat anti-rabbit (LI-COR Biosciences).

Chemical reagents used include emetine (Sigma-Aldrich), CB5083 (Cleave Biosciences and Cayman Chemical), MLN7243 (Chemietek), MG132 (Selleck Chemicals), and Bortezomib (Cell Signaling Technologies).

Cell culture, transfections, and stable cell line generation

HepG2 cells (American Type Culture Collection) were cultured in Roswell Park Memorial Institute 1640 (RPMI; Thermo Fisher Scientific) or DMEM containing 4.5 g/l glucose and L-glutamine (Corning) supplemented with 10% fetal bovine serum (FBS; Thermo Fisher Scientific and Gemini Bio Products) at 37°C and 5% CO_2. Stable HEK293 cells expressing S-tagged Hrd1 (To *et al.*, 2017) were grown in DMEM supplemented with 10% FBS at 37°C and 5% CO_2.

Cells at 60–80% confluence were transfected with the indicated plasmids using XtremeGENE HP DNA transfection reagent (Sigma-Aldrich) following the manufacturer's protocols. Depletion of SCD1 in HepG2 cells was accomplished by transfection of SCD1-targeting siRNAs from Sigma-Aldrich using RNAiMAX Lipofectamine reagent (Thermo Fisher Scientific). siRNA sequences targeting SCD1 include 5′-GAUAUGCUGUGGUGCUUAA-3′ (siRNA1), 5′-GAUAUCGUCCUUAUGACAA-3′ (siRNA2), 5′-GACGAUAUCUCUAGCUCCU-3′ (siRNA3), and 5′-GUGAGUACCGCUGGCACAU-3′ (siRNA4). MISSION siRNA Universal Negative Control #1 (SIC001) was used as the control siRNA.

Differential fractionation

Cultured cells were collected, washed with ice-cold phosphate-buffered saline (PBS), and incubated in hypotonic lysis medium (HLM: 20 mM Tris-HCl, pH 7.4, 1 mM EDTA) supplemented with 10 mM N-ethylmaleimide (NEM; Thermo Fisher Scientific) on ice for 10 min. Cells were then transferred to a 7-ml chilled glass dounce homogenizer and dounced using a tight pestle for 40 strokes. Samples were centrifuged (500 × *g*, 5 min, two times) to remove unbroken cells. The remaining supernatant was then centrifuged (20,000 × *g*, 30 min at 4°C) to separate heavy membrane and cytosolic fractions. The resulting pellet (membrane) was then reconstituted to its corresponding cytosolic fraction volume using either HLM buffer (for immunoblotting) or 8M urea lysis buffer (for diGly enrichment, details below). For immunoblotting, SDS was then added to achieve a final detergent concentration of 1% and equal volumes were analyzed.

Affinity purification

Cells were collected and washed twice using ice-cold PBS. Cells were resuspended in immunoprecipitation (IP) lysis buffer (50 mM Tris-HCl, pH 7.5, 150 mM NaCl, 1% digitonin [EMD Millipore]) containing protease inhibitor tablets (Thermo Fisher Scientific) and gently rotated for 30 min at 4°C. Lysates were centrifuged (20,000 × *g*, 10 min) and soluble protein (supernatant) transferred to new tubes. Supernatant protein concentration was then determined using the BCA assay (Thermo Fisher Scientific) according to the manufacturer's instructions.

S-protein agarose bead slurry (25 µl bead bed/mg lysate; EMD Millipore) was washed two times with IP lysis buffer followed by one time with IP buffer containing 1% digitonin. Beads were then mixed with equivalent amounts of supernatant (2 h rotating, 4°C), washed three times with IP lysis buffer containing 0.1% digitonin, and proteins eluted with Laemmli buffer for immunoblotting. Where indicated, affinity-purified proteins were treated with 1 µg of USP2cc (Boston Biochem) for 1 h at 37°C before elution from the beads.

Immunoblotting

Cells were washed with PBS and lysed in 1% SDS. Protein quantity was determined using a bicinchoninic acid assay (Thermo Fisher Scientific). Normalized cell lysates in Laemmli sample buffer were heated at 65°C for 5 min and resolved on 4–20% SDS–PAGE gradient gels (Bio-Rad Laboratories). Gels were transferred to nitrocellulose membrane (Bio-Rad Laboratories), blocked in PBS containing 0.1% Tween-20 (PBST) and 5% milk, and then incubated with primary antibody for either 2 h at room temperature or overnight at 4°C. Blots were then washed and incubated with secondary antibodies in PBST. Following washing PBST, blots were visualized using the LI-COR Odyssey Imaging System. Densitometry analyses were performed using the UN-SCAN-IT gel analysis (version 6.1; Silk Scientific) or ImageJ (version 1.49b; National Institutes of Health, Bethesda, MD) software.

Enrichment of diGly-modified peptides

Cells were cultured in SILAC DMEM lacking lysine and arginine, supplemented with 10% dialyzed FBS and the appropriate amino acids: light media—L-arginine (Arg0) and L-lysine (Lys0; Sigma-Aldrich) or heavy media—L-arginine (Arg0) and $^{13}C_6{}^{15}N_2$-L-lysine (Lys8; Cambridge Isotope Laboratories). Samples were then processed for diGly immunopurification (Kim *et al.*, 2011). Following a 6 h treatment with DMSO (light) or 5 µM CB5083 (heavy), membrane fractions were collected, solubilized in urea lysis buffer (8 M urea, 50 mM Tris-HCl, pH 8.0, 50 mM NaCl), reduced with 10 mM dithiothreitol (Thermo Fisher Scientific), and alkylated with 25 mM iodoacetamide (Thermo Fisher Scientific). Equal amounts of protein totaling 5–10 mg from the membrane fractions were combined, diluted with 50 mM Tris-HCl, pH 8.0, 4 M urea, and digested overnight with 2 µg/mg LysC (Wako Laboratory Chemicals). Proteins were further diluted to 1.6 M urea and digested for 24 h with 10 µg/mg mass spectrometry grade trypsin (Thermo Fisher Scientific).

Digested peptides were desalted via Sep-Pak C18 6-cc cartridges (Waters) and lyophilized. Samples were then immunoprecipitated using a PTMScan Ubiquitin remnant Motif (K-ε-GG) Kit (Cell Signaling Technologies) according to the manufacturer's protocols. Briefly, lyophilized peptides were dissolved in IAP buffer (50 mM MOPS/NaOH, pH 7.2, 10 mM Na_2HPO_4, and 50 mM NaCl) and cleared by centrifugation at 10,000 × *g* for 5 min. For each independent experiment, one tube of K-ε-GG antibody bead conjugates were washed four times with PBS, and clarified peptides were incubated with the beads for at least 2 h with gentle agitation. Beads were washed two times with IAP buffer and three times with MilliQ water and eluted twice with 0.15% trifluoroacetic acid. Eluted peptides were desalted using C18 StageTips (Thermo Fisher Scientific), dried using a Speedvac, and resuspended in 0.1% formic acid (Sigma-Aldrich) for analysis by tandem mass spectrometry (LC-MS/MS).

LC-MS/MS analysis

Digested peptides were analyzed by LC-MS/MS on a Q Exactive Orbitrap mass spectrometer (Thermo Fisher Scientific) in conjunction with Proxeon Easy-nLC II HPLC (Thermo Fisher Scientific) and a Proxeon nanospray source at the UC Davis Proteomics Core Facility as described (To *et al*., 2017). The resulting MS/MS raw spectral data were analyzed using the MaxQuant software platform (version 1.5.1.0; Cox and Mann, 2008), employing the full UniProt human protein sequence database to obtain diGly-modified peptide SILAC ratios. A reversed-protein decoy search strategy was also employed to minimize false discovery rate. All mass spectrometry files are available through the Proteomics Identifications (PRIDE) database (Project accession: PXD008842).

Bioinformatic analyses

GO analysis of candidate ERAD substrates was performed using the Database for Annotation, Visualization and Integrated Discovery (DAVID) v6.8 (Supplemental Table S3; Huang *et al*., 2009). REVIGO (Supek *et al*., 2011) was then used to simplify and visualize the GO terms and the Benjamini corrected *p* values. GO networks were exported from REVIGO and the final networks generated using Cytoscape (Shannon *et al*., 2003). Protein localization and topology listed in Supplemental Table S2 were based on UNIPROT annotations.

Generation of RNF5 knockout cells

RNF5 knockout lines were generated using the targeting sequence 5′-CGCTCGCGATTTGGCCCTTC-3′ cloned into PX459 (Addgene; plasmid #48139) transfected into HEK293 cells. PX459 without a targeting sequence was transfected as a control. Transfected cells were selected with 1 µg/ml puromycin (Sigma-Aldrich) for at least 1 wk. Clonal cell lines were isolated by limited dilution and screened for knockout by immunoblotting.

ACKNOWLEDGMENTS

This research was supported by grants from the National Institutes of Health (No. R21AG056502 and No. R01GM112948 to J.A.O. and No. F32GM119380 to E.H.). We thank Kirill Bersuker for a critical reading of the manuscript and Michelle Salemi at the UC Davis Proteomics Core Facility for technical assistance.

REFERENCES

Anderson DJ, Le Moigne R, Djakovic S, Kumar B, Rice J, Wong S, Wang J, Yao B, Valle E, Kiss von Soly S, *et al*. (2015). Targeting the AAA ATPase p97 as an approach to treat cancer through disruption of protein homeostasis. Cancer Cell 28, 653–665.

Bagola K, Mehnert M, Jarosch E, Sommer T (2011). Protein dislocation from the ER. Biochim Biophys Acta 1808, 925–936.

Bersuker K, Peterson CWH, To M, Sahl SJ, Savikhin V, Grossman EA, Nomura DK, Olzmann JA (2018). A proximity labeling strategy provides insights into the composition and dynamics of lipid droplet proteomes. Dev Cell 44, 97–112.e7.

Blythe EE, Olson KC, Chau V, Deshaies RJ (2017). Ubiquitin- and ATP-dependent unfoldase activity of P97/VCP•NPLOC4•UFD1L is enhanced by a mutation that causes multisystem proteinopathy. Proc Natl Acad Sci USA 114, E4380–E4388.

Bodnar NO, Rapoport TA (2017). Molecular mechanism of substrate processing by the cdc48 atpase complex. Cell 169, 722–735.

Braun S, Matuschewski K, Rape M, Thoms S, Jentsch S (2002). Role of the ubiquitin-selective CDC48(UFD1/NPL4)chaperone (segregase) in ERAD of OLE1 and other substrates. EMBO J 21, 615–621.

Carvalho P, Goder V, Rapoport TA (2006). Distinct ubiquitin-ligase complexes define convergent pathways for the degradation of ER proteins. Cell 126, 361–373.

Christianson JC, Olzmann JA, Shaler TA, Sowa ME, Bennett EJ, Richter CM, Tyler RE, Greenblatt EJ, Harper JW, Kopito RR (2011). Defining human ERAD networks through an integrative mapping strategy. Nat Cell Biol 14, 93–105.

Christianson JC, Shaler TA, Tyler RE, Kopito RR (2008). OS-9 and GRP94 deliver mutant α1-antitrypsin to the Hrd1-SEL1L ubiquitin ligase complex for ERAD. Nat Cell Biol 10, 272–282.

Christianson JC, Ye Y (2014). Cleaning up in the endoplasmic reticulum: ubiquitin in charge. Nat Struct Mol Biol 21, 325–335.

Cox J, Mann M (2008). MaxQuant enables high peptide identification rates, individualized p.p.b.-range mass accuracies and proteome-wide protein quantification. Nat Biotechnol 26, 1367–1372.

Ernst R, Claessen JHL, Mueller B, Sanyal S, Spooner E, van der Veen AG, Kirak O, Schlieker CD, Weihofen WA, Ploegh HL (2011). Enzymatic blockade of the ubiquitin-proteasome pathway. PLoS Biol 8, e1000605.

Fisher E, Lake E, McLeod RS (2014). Apolipoprotein B100 quality control and the regulation of hepatic very low density lipoprotein secretion. J Biomed Res 28, 178–193.

Foresti O, Rodriguez-Vaello V, Funaya C, Carvalho P (2014). Quality control of inner nuclear membrane proteins by the Asi complex. Science 346, 751–755.

Foresti O, Ruggiano A, Hannibal-Bach HK, Ejsing CS, Carvalho P (2013). Sterol homeostasis requires regulated degradation of squalene monooxygenase by the ubiquitin ligase Doa10/Teb4. Elife 2, e00953.

Gao D, Inuzuka H, Tan MK, Fukushima H, Locasale JW, Liu P, Wan L, Zhai B, Chin YR, Shaik S, *et al*. (2011). mTOR drives its own activation via SCF(βTrCP)-dependent degradation of the mTOR inhibitor DEPTOR. Mol Cell 44, 290–303.

Gendron JM, Webb K, Yang B, Rising L, Zuzow N, Bennett EJ (2016). Using the ubiquitin-modified proteome to monitor distinct and spatially restricted protein homeostasis dysfunction. Mol Cell Proteomics 15, 2576–2593.

Gill S, Stevenson J, Kristiana I, Brown AJ (2011). Cholesterol-dependent degradation of squalene monooxygenase, a control point in cholesterol synthesis beyond HMG-CoA reductase. Cell Metab 13, 260–273.

Ginsberg HN, Fisher EA (2009). The ever-expanding role of degradation in the regulation of apolipoprotein B metabolism. J Lipid Res 50(Suppl), S162–S166.

Grove DE, Fan C-Y, Ren HY, Cyr DM (2011). The endoplasmic reticulum-associated Hsp40 DNAJB12 and Hsc70 cooperate to facilitate RMA1 E3-dependent degradation of nascent CFTRDeltaF508. Mol Biol Cell 22, 301–314.

Guerriero CJ, Brodsky JL (2012). The delicate balance between secreted protein folding and endoplasmic reticulum-associated degradation in human physiology. Physiol Rev 92, 537–576.

Harper JW, Tan MK (2012). Understanding cullin-RING E3 biology through proteomics-based substrate identification. Mol Cell Proteomics 11, 1541–1550.

Hegde RS, Ploegh HL (2010). Quality and quantity control at the endoplasmic reticulum. Curr Opin Cell Biol 22, 437–446.

Hitchcock AL, Auld K, Gygi SP, Silver PA (2003). A subset of membrane-associated proteins is ubiquitinated in response to mutations in the endoplasmic reticulum degradation machinery. Proc Natl Acad Sci USA 100, 12735–12740.

Hoppe T, Matuschewski K, Rape M, Schlenker S, Ulrich HD, Jentsch S (2000). Activation of a membrane-bound transcription factor by regulated ubiquitin/proteasome-dependent processing. Cell 102, 577–586.

Hosokawa N, Wada I, Nagasawa K, Moriyama T, Okawa K, Nagata K (2008). Human XTP3-B forms an endoplasmic reticulum quality control scaffold with the HRD1-SEL1L ubiquitin ligase complex and BiP. J Biol Chem 283, 20914–20924.

Huang DW, Sherman BT, Lempicki RA (2009). Systematic and integrative analysis of large gene lists using DAVID bioinformatics resources. Nat Protoc 4, 44–57.

Jeon YJ, Khelifa S, Ratnikov B, Scott DA, Feng Y, Parisi F, Ruller C, Lau E, Kim H, Brill LM, *et al*. (2015). Regulation of glutamine carrier proteins by RNF5 determines breast cancer response to ER stress-inducing chemotherapies. Cancer Cell 27, 354–369.

Ji Y, Kim H, Yang L, Sha H, Roman CA, Long Q, Qi L (2016). The Sel1L-Hrd1 endoplasmic reticulum-associated degradation complex manages a key checkpoint in B cell development. Cell Rep 16, 2630–2640.

Jo Y, Debose-Boyd RA (2010). Control of cholesterol synthesis through regulated ER-associated degradation of HMG CoA reductase. Crit Rev Biochem Mol Biol 45, 185–198.

Kato H, Sakaki K, Mihara K (2006). Ubiquitin-proteasome-dependent degradation of mammalian ER stearoyl-CoA desaturase. J Cell Sci 119, 2342–2353.

Kim W, Bennett EJ, Huttlin EL, Guo A, Li J, Possemato A, Sowa ME, Rad R, Rush J, Comb MJ, *et al*. (2011). Systematic and quantitative assessment of the ubiquitin-modified proteome. Mol Cell 44, 325–340.

Kirkpatrick DS, Weldon SF, Tsaprailis G, Liebler DC, Gandolfi AJ (2005). Proteomic identification of ubiquitinated proteins from human cells expressing His-tagged ubiquitin. Proteomics 5, 2104–2111.

Kuang E, Okumura CYM, Sheffy-Levin S, Varsano T, Shu VC-W, Qi J, Niesman IR, Yang H-J, López-Otín C, Yang WY, *et al*. (2012). Regulation of ATG4B stability by RNF5 limits basal levels of autophagy and influences susceptibility to bacterial infection. PLoS Genet 8, e1003007.

Lee JN, Gong Y, Zhang X, Ye J (2006). Proteasomal degradation of ubiquitinated Insig proteins is determined by serine residues flanking ubiquitinated lysines. Proc Natl Acad Sci USA 103, 4958–4963.

Liu T-F, Tang J-J, Li P-S, Shen Y, Li J-G, Miao H-H, Li B-L, Song B-L (2012). Ablation of gp78 in liver improves hyperlipidemia and insulin resistance by inhibiting SREBP to decrease lipid biosynthesis. Cell Metab 16, 213–225.

Mark KG, Loveless TB, Toczyski DP (2016). Isolation of ubiquitinated substrates by tandem affinity purification of E3 ligase-polyubiquitin-binding domain fusions (ligase traps). Nat Protoc 11, 291–301.

Mark KG, Simonetta M, Maiolica A, Seller CA, Toczyski DP (2014). Ubiquitin ligase trapping identifies an SCF(Saf1) pathway targeting unprocessed vacuolar/lysosomal proteins. Mol Cell 53, 148–161.

Matsuda N, Suzuki T, Tanaka K, Nakano A (2001). Rma1, a novel type of RING finger protein conserved from Arabidopsis to human, is a membrane-bound ubiquitin ligase. J Cell Sci 114, 1949–1957.

Morito D, Hirao K, Oda Y, Hosokawa N, Tokunaga F, Cyr DM, Tanaka K, Iwai K, Nagata K (2008). Gp78 cooperates with RMA1 in endoplasmic reticulum-associated degradation of CFTRΔF508. Mol Biol Cell 19, 1328–1336.

Mziaut H, Korza G, Ozols J (2000). The N terminus of microsomal Δ9 stearoyl-CoA desaturase contains the sequence determinant for its rapid degradation. Proc Natl Acad Sci USA 97, 8883–8888.

Na CH, Jones DR, Yang Y, Wang X, Xu Y, Peng J (2012). Synaptic protein ubiquitination in rat brain revealed by antibody-based ubiquitome analysis. J Proteome Res 11, 4722–4732.

Needham PG, Brodsky JL (2013). How early studies on secreted and membrane protein quality control gave rise to the ER associated degradation (ERAD) pathway: the early history of ERAD. Biochim Biophys Acta 1833, 2447–2457.

Ntambi JM, Miyazaki M (2003). Recent insights into stearoyl-CoA desaturase-1. Curr Opin Lipidol 14, 255–261.

O'Connor HF, Lyon N, Leung JW, Agarwal P, Swaim CD, Miller KM, Huibregtse JM (2015). Ubiquitin-activated interaction traps (UBAITs) identify E3 ligase binding partners. EMBO Rep 16, 1699–1712.

Olzmann JA, Kopito RR, Christianson JC (2013). The mammalian endoplasmic reticulum-associated degradation system. Cold Spring Harb Perspect Biol 5, a013185.

Ordureau A, Münch C, Harper JW (2015). Quantifying ubiquitin signaling. Mol Cell 58, 660–676.

Peng J, Schwartz D, Elias JE, Thoreen CC, Cheng D, Marsischky G, Roelofs J, Finley D, Gygi SP (2003). A proteomics approach to understanding protein ubiquitination. Nat Biotechnol 21, 921–926.

Prabhu AV, Luu W, Sharpe LJ, Brown AJ (2016). Cholesterol-mediated degradation of 7-dehydrocholesterol reductase switches the balance from cholesterol to vitamin D synthesis. J Biol Chem 291, 8363–8373.

Qi L, Tsai B, Arvan P (2017). New insights into the physiological role of endoplasmic reticulum-associated degradation. Trends Cell Biol 27, 430–440.

Ramanathan HN, Ye Y (2012). The p97 ATPase associates with EEA1 to regulate the size of early endosomes. Cell Res 22, 346–359.

Rape M, Hoppe T, Gorr I, Kalocay M, Richly H, Jentsch S (2001). Mobilization of processed, membrane-tethered SPT23 transcription factor by CDC48(UFD1/NPL4), a ubiquitin-selective chaperone. Cell 107, 667–677.

Ruggiano A, Foresti O, Carvalho P (2014). Quality control: ER-associated degradation: protein quality control and beyond. J Cell Biol 204, 869–879.

Shannon P, Markiel A, Ozier O, Baliga NS, Wang JT, Ramage D, Amin N, Schwikowski B, Ideker T (2003). Cytoscape: a software environment for integrated models of biomolecular interaction networks. Genome Res 13, 2498–2504.

Shi G, Somlo DR, Kim GH, Prescianotto-Baschong C, Sun S, Beuret N, Long Q, Rutishauser J, Arvan P, Spiess M, *et al*. (2017). ER-associated degradation is required for vasopressin prohormone processing and systemic water homeostasis. J Clin Invest 127, 3897–3912.

Shimizu Y, Okuda-Shimizu Y, Hendershot LM (2010). Ubiquitylation of an ERAD substrate occurs on multiple types of amino acids. Mol Cell 40, 917–926.

Song BL, Sever N, DeBose-Boyd RA (2005). Gp78, a membrane-anchored ubiquitin ligase, associates with Insig-1 and couples sterol-regulated ubiquitination to degradation of HMG CoA reductase. Mol Cell 19, 829–840.

Stevenson J, Huang EY, Olzmann JA (2016). Endoplasmic reticulum-associated degradation and lipid homeostasis. Annu Rev Nutr 36, 511–542.

Supek F, Bošnjak M, Škunca N, Šmuc T (2011). REVIGO summarizes and visualizes long lists of gene ontology terms. PLoS One 6, e21800.

Tan MK, Lim HJ, Bennett EJ, Shi Y, Harper JW (2013). Parallel SCF adaptor capture proteomics reveals a role for SCFFBXL17 in NRF2 activation via BACH1 repressor turnover. Mol Cell 52, 9–24.

Tan MK, Lim HJ, Harper JW (2011). SCF(FBXO22) regulates histone H3 lysine 9 and 36 methylation levels by targeting histone demethylase KDM4A for ubiquitin-mediated proteasomal degradation. Mol Cell Biol 31, 3687–3699.

To M, Peterson CWH, Roberts MA, Counihan JL, Wu TT, Forster MS, Nomura DK, Olzmann JA (2017). Lipid disequilibrium disrupts ER proteostasis by impairing ERAD substrate glycan trimming and dislocation. Mol Biol Cell 28, 270–284.

Tsai YC, Mendoza A, Mariano JM, Zhou M, Kostova Z, Chen B, Veenstra T, Hewitt SM, Helman LJ, Khanna C, Weissman AM (2007). The ubiquitin ligase gp78 promotes sarcoma metastasis by targeting KAI1 for degradation. Nat Med 13, 1504–1509.

Tyler RE, Pearce MMP, Shaler TA, Olzmann JA, Greenblatt EJ, Kopito RR (2012). Unassembled CD147 is an endogenous endoplasmic reticulum-associated degradation substrate. Mol Biol Cell 23, 4668–4678.

Udeshi ND, Mani DR, Eisenhaure T, Mertins P, Jaffe JD, Clauser KR, Hacohen N, Carr SA (2012). Methods for quantification of in vivo changes in protein ubiquitination following proteasome and deubiquitinase inhibition. Mol Cell Proteomics 11, 148–159.

Wojcikiewicz RJH, Pearce MMP, Sliter DA, Wang Y (2009). When worlds collide: IP(3) receptors and the ERAD pathway. Cell Calcium 46, 147–153.

Yen HC, Elledge SJ (2008). Identification of SCF ubiquitin ligase substrates by global protein stability profiling. Science 322, 923–929.

Yen HC, Xu Q, Chou DM, Zhao Z, Elledge SJ (2008). Global protein stability profiling in mammalian cells. Science 322, 918–923.

Ye Y, Tang WK, Zhang T, Xia D (2017). A mighty "protein extractor" of the cell: structure and function of the p97/CDC48 ATPase. Front Mol Biosci 4, 39.

Younger JM, Chen L, Ren H-Y, Rosser MFN, Turnbull EL, Fan C-Y, Patterson C, Cyr DM (2006). Sequential quality-control checkpoints triage misfolded cystic fibrosis transmembrane conductance regulator. Cell 126, 571–582.

Zhong B, Zhang Y, Tan B, Liu T-T, Wang Y-Y, Shu H-B (2010). The E3 ubiquitin ligase RNF5 targets virus-induced signaling adaptor for ubiquitination and degradation. J Immunol 184, 6249–6255.